Engineering 53 (2025) 176–186

Contents lists available at ScienceDirect

Engineering

journal homepage: www.elsevier.com/locate/eng

Research
Unconventional and Intelligent Oil & Gas Engineering—Article

A Potential Commercialization Method for Gas Production from Off-Shore Hydrate Reservoirs

Baojiang Sun [a,b,*], Jinsheng Sun [a,b], Youqiang Liao [c], Miao Dong [d], Jie Zhong [a,b], Praveen Linga [e,*]

[a] School of Petroleum Engineering, China University of Petroleum (East China), Qingdao 266580, China
[b] State Key Laboratory of Deep Oil and Gas, China University of Petroleum (East China), Qingdao 266580, China
[c] State Key Laboratory of Geomechanics and Geotechnical Engineering Safety, Institute of Rock and Soil Mechanics, Chinese Academy of Sciences, Wuhan 430071, China
[d] Key Laboratory of Deep Petroleum Intelligent Exploration and Development, Institute of Geology and Geophysics, Chinese Academy of Sciences, Beijing 100029, China
[e] Department of Chemical and Biomolecular Engineering, National University of Singapore, Singapore 117582, Singapore

ARTICLE INFO

Article history:
Received 19 December 2024
Revised 21 March 2025
Accepted 23 April 2025
Available online 27 April 2025

Keywords:
Hydrate exploitation
Looping wells
Geothermal coupling with depressurization
Commercialization

ABSTRACT

Depressurization and heat injection are viewed as the main methods to be used in natural gas hydrate (NGH) exploitation. However, these methods have limitations, such as low energy-utilization efficiency or a limited extraction range, and are still far from commercial exploitation. In this work, we propose a potential commercial method to exploit NGHs by effectively using geothermal energy inside deep reservoirs. Specifically, a loop well structure is designed to economically extract geothermal energy. Based on an analysis of our developed model, when the looping well is coupled with depressurization, the profits of high NGH production can surpass the drilling costs of extracting geothermal energy. Moreover, as the temperature of fluids from the geothermal layer exceeds 62 °C, the fluid heat is mainly consumed by the rock matrix of the hydrate formation, instead of promoting NGH dissociation. Based on this threshold temperature, a loop well drilled to a depth of about 4000 m for hydrate sediment in the Shenhu area of the South China Sea would be able to efficiently extract geothermal energy, leading to an approximate 73% increase in gas production in comparison with conventional depressurization. An economic analysis suggests that our proposed method can reduce the exploitation cost of methane to 0.46 USD·m^{-3}. Furthermore, as the hydrate saturation increases to 0.5, the exploitation cost can be further reduced to 0.14 USD·m^{-3}. Overall, a looping well coupled with geothermal energy and depressurization is expected to pave the way for commercial NGH exploitation.

© 2025 THE AUTHORS. Published by Elsevier LTD on behalf of Chinese Academy of Engineering and Higher Education Press Limited Company. This is an open access article under the CC BY-NC-ND license (http://creativecommons.org/licenses/by-nc-nd/4.0/).

1. Introduction

With current population growth and industrial development, the increasing consumption of fossil fuels is causing serious environmental issues; in turn, the need to address these issues is stimulating rapid development in low-carbon and clean energy [1–4]. Research indicates that the global reserves of natural gas hydrates (NGHs) are approximately 3000 to 20 000 trillion m^3, with a total organic carbon content roughly double that of conventional fossil fuels [4,5]. In this regard, NGHs have garnered increasing global attention as a potentially environmentally friendly and widely distributed resource [6]. Many methods have been developed to explore NGH deposits, including thermal stimulation [7], depressurization [8], carbon dioxide (CO_2) replacement [9], and inhibitor injection [10]. However, each of these methods carries its own inherent technical flaws, such as low energy-utilization efficiency, limited extraction range, low gas production, and high production cost [11,12]. Consequently, the efficient and economical exploration of this clean energy source has become a frontier topic in this research area.

The reservoir properties and gas production characteristics of NGHs preclude the use of many conventional extraction methods employed in petroleum/natural gas production. To date, eight hydrate production tests have been conducted globally in both permafrost and offshore marine regions—including the Mallik [13], Ignik Sikumi [14], Nankai Trough [15,16], and Shenhu area [17–20]—utilizing thermal stimulation, gas exchange, and depressurization. Field tests have indicated that depressurization holds the

* Corresponding authors.
E-mail addresses: sunbj1128@vip.126.com (B. Sun), chepl@nus.edu.sg (P. Linga).

https://doi.org/10.1016/j.eng.2025.04.016
2095-8099/© 2025 THE AUTHORS. Published by Elsevier LTD on behalf of Chinese Academy of Engineering and Higher Education Press Limited Company.
This is an open access article under the CC BY-NC-ND license (http://creativecommons.org/licenses/by-nc-nd/4.0/).

greatest potential for destabilizing hydrate sediments. However, because hydrate dissociation requires substantial amounts of heat and is constrained by the poor thermal conductivity of the reservoir, solely relying on the inherent energy of the formation often leads to a sharp decline in gas production rates [5,21,22]—a phenomenon that was evidenced in the two marine hydrate production tests conducted thus far. Additionally, increasing the degree of depressurization to boost production often results in issues such as sand production and secondary hydrate formation [23]. Thus, energy supply remains one of the most critical challenges in the development of gas hydrates and is considered the key factor determining the feasibility of NGH commercial exploitation [24].

Against this background, various methods have been proposed to supply energy during hydrate development, including auxiliary electrical heating [25], injections of hot water [26], steam [27], and self-heating solids [28]. Experiments and simulations have been conducted to explain the mechanisms and effects of these methods on gas production enhancement. However, establishing a comprehensive heat-supplementation system that minimizes secondary costs remains a significant constraint on the application of these methods. Some researchers [29] have also explored the use of geothermal energy for energy supplementation; however, optimizing the utilization of geothermal energy to overcome the substantial drilling and operational costs presents a formidable theoretical challenge. Despite the potential of geothermal energy to drive hydrate dissociation, the effectiveness of this energy in low-temperature seabed environments—where a significant portion of the energy might dissipate into the surrounding environment rather than being utilized for hydrate dissociation—requires in-depth investigation.

The rapid development of the petroleum industry [30,31], coupled with the maturation of technologies such as horizontal drilling, sidetracking, and rotary steerable systems, has made complex extraction well structures a reality [32]. For example, in 2020, the second gas hydrate production test in the Shenhu area of the South China Sea employed horizontal well technology for the first time, significantly increased the gas production rate and cumulative gas yield from the hydrate deposits [17]. Therefore, improving gas production capacity from an operational perspective is also a viable pathway for the commercial exploitation of gas hydrates [33].

Although Sun et al. [34] and a few previous research [29] have proposed the idea of utilizing geothermal energy for gas hydrate development and demonstrated its effectiveness to enhance gas production through numerical simulations, these studies have not considered the well construction costs in conjunction with real geological conditions. Building upon this concept, this study aims to construct a novel hydrate development well configuration. This configuration includes a geothermal well, a heat-injection well, and a production well, forming a hydrate development scheme that combines depressurization and heat injection. The core concept involves harnessing geothermal energy from abandoned oil and gas wells and injecting this thermal energy into hydrate reservoirs. This innovative approach aims to leverage geothermal energy to efficiently dissociate the hydrate and enhance gas production.

To evaluate the performance of this novel method, a comprehensive model and a complete numerical solution methodology for gas hydrate development are constructed. Utilizing the geological conditions of the Shenhu area in the South China Sea, which includes hydrate deposits and deep high-temperature geothermal layers, a series of numerical simulations are conducted. Thereafter, the geothermal energy exploitation characteristics and fluid production behaviors of this novel hydrate production method are quantitatively evaluated. A further analysis of the effects of costs, hydrate reservoir conditions, and gas production rate on the commercialization potential is also included. Overall, this work provides an in-depth understanding of the roles geothermal energy and a loop well structure can play in hydrate decomposition. Moreover, the developed numerical model for NGH development can act as a powerful tool to evaluate and optimize NGH exploitation strategies and maximize NGH recovery.

2. Enhanced gas production from a hydrate reservoir

As illustrated in Fig. 1, the basic principle of the novel loop well method for NGH extraction involves using a low-temperature fluid to harvest geothermal energy from deep formations and injecting it into the hydrate reservoir to enhance the dissociation kinetics of the hydrates, thereby increasing the NGH production capacity. This system comprises a heat-extraction well, a heat-injection well, and a production well, with the heat-extraction and heat-injection wells being connected end-to-end to form a loop well system for heat extraction and injection.

In this system, a low-temperature heat-extraction medium (i.e., seawater, CO_2, or a specially formulated dissociation-promoting fluid) is injected into heat-extraction well. The heat-extraction fluid undergoes extensive heat exchanges with the high-temperature sediment in the long horizontal section at depth, gradually increasing in temperature. It then flows back up the wellbore, with the pressure being adjusted via a throttle control valve, before entering the heat-injection well. Excess water is cycled back to the platform for reinjection.

Initially, the heat-injection well can also function as a production well during the depressurization development. Once the gas production rate declines to a certain level, the well is converted to a heat-injection well for hot water injection development. This approach maximizes the utilization of the inherent geothermal energy of the formation to increase the gas production efficiency. Moreover, after a period of depressurization, the hydrate saturation around the well decreases and the permeability significantly increases, making the hot water injection more effective [35,36]. By integrating this loop well system with an existing geothermal resource, this method leverages both the depressurization and thermal-stimulation techniques to optimize gas hydrate production, offering a promising strategy for the commercial development of hydrate resources.

Compared with previously proposed closed heat-injection systems, the loop well hydrate-extraction system offers the dual advantages of controlling both the fluid temperatures and the injection pressures. Before the heat-carrying fluid enters the hydrate layer, precise regulation of the injection pressure is achieved through a throttle control valve [37]. In addition, since the heat-injection well in the loop well system is open, excess fluid can directly return to the platform, allowing for precise control over the flow rate of the heat-transfer medium within the system. The fluid flow rate determines the heat exchange efficiency in the high-temperature geothermal layer, thereby controlling the temperature of the injected fluid. In contrast, closed heat-injection systems rely on the permeability of the hydrate reservoir to determine the overall flow rate if the injection pressure is controlled [27]. For the ultra-low-permeability hydrate reservoirs in the South China Sea, when the flow rate in the wellbore is very low, the heat carried by the transfer medium is likely to be lost to the low-temperature formation before it enters the heat-injection well [38,39]. This inefficiency is mitigated in the loop well system, where the flow rate can be finely adjusted to optimize heat exchange and maintain the desired fluid temperature as it reaches the hydrate reservoir, thereby increasing the overall effectiveness of the hydrate dissociation process.

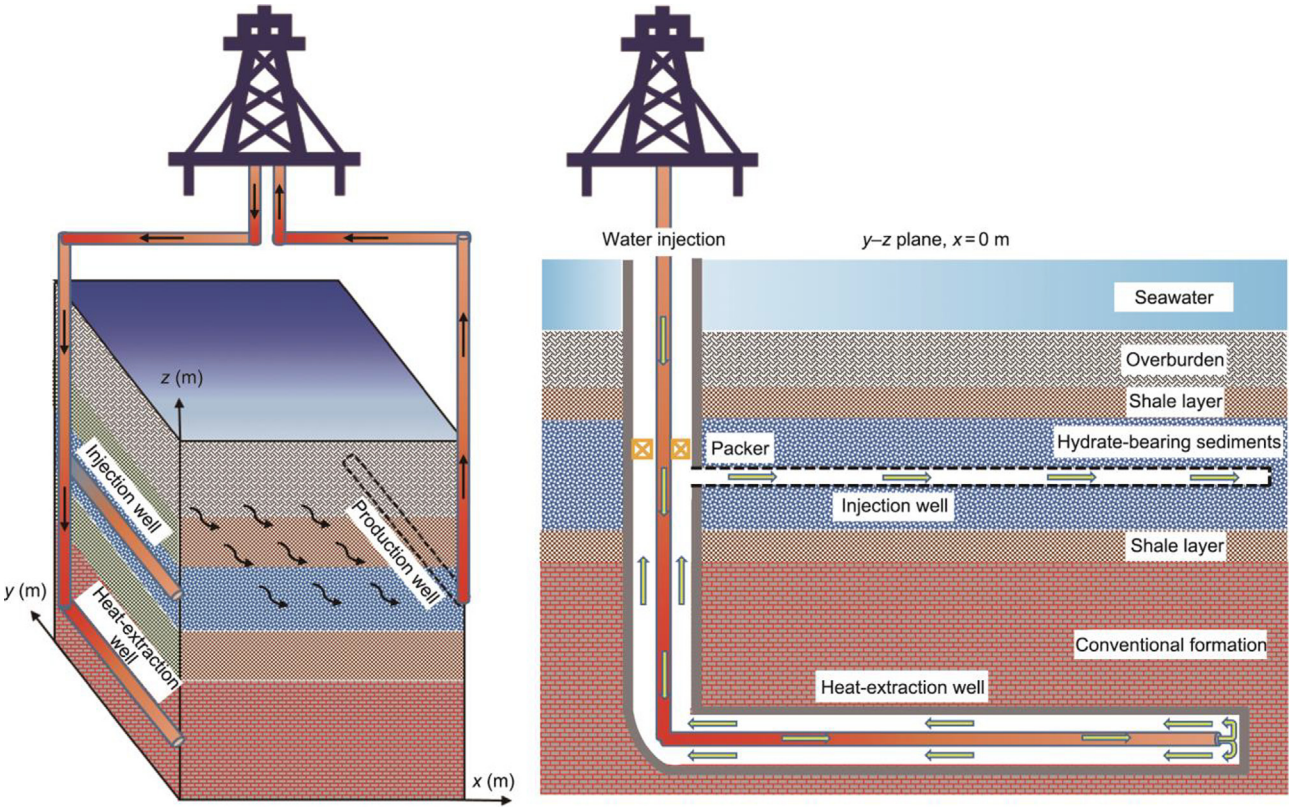

Fig. 1. Principles of hydrate production with geothermal energy via cycling water in a looping well system.

3. Modeling approach

In this new enhanced hydrate-development system, the focus is on the single-phase water flow in the geothermal wells and injection wells, the multiphase flow within the hydrate reservoir and production wellbore, and the heat transfer and hydrate decomposition throughout the entire flow process. In this section, we develop a comprehensive hydrate-development model encompassing the fluid flow, heat transfer, and hydrate decomposition.

3.1. Fluid flow

The hydrate reservoir's pore space is saturated with three phases: hydrate, water, and free gas. Assuming that hydrate particles do not migrate within the porous media, the continuity equations for free gas, water, and hydrate within the porous medium can be expressed based on the principle of mass conservation, as follows:

$$\frac{\partial(\phi_{wg}\rho_w S_w)}{\partial t}+\nabla\cdot\left(-\rho_w\frac{\boldsymbol{k}k_{rw}}{\mu_w}(\nabla p_w+\rho_w\boldsymbol{g})\right)=\dot{m}_w \tag{1}$$

$$\frac{\partial\left(\phi_{wg}\rho_g S_g\right)}{\partial t}+\nabla\cdot\left(-\rho_g\frac{\boldsymbol{k}k_{rg}}{\mu_g}\left(\nabla p_g+\rho_g\boldsymbol{g}\right)\right)=\dot{m}_g \tag{2}$$

$$\frac{\partial(\phi\rho_h S_h)}{\partial t}=\dot{m}_h \tag{3}$$

where ϕ is the porosity and ϕ_{wg} is the effective porosity of the hydrate-bearing sediments, $\phi_{wg}=\phi(1-S_h)$; S, ρ, and p are the saturation, density, and pressure, respectively; the subscripts h, g, and w denote hydrate, gas, and water, respectively; t is the time, in s; $\boldsymbol{k}$ is the absolute permeability of the hydrate-bearing sediments, in m^2; k_{rw} and k_{rg} are the relative permeabilities of water and gas in the porous media, respectively; μ_w and μ_g are the viscosities of water and gas, respectively, in Pa·s; $\boldsymbol{g}$ is the gravitational acceleration, in $m\cdot s^{-2}$; $\dot{m}_g$ and $\dot{m}_w$ are the rate of gas and water generation induced by hydrate decomposition, respectively, in $kg\cdot(m^3\cdot s)^{-1}$; and $\dot{m}_h$ is the decomposition rate of the hydrate, which is mainly related to the temperature, pressure, and specific surface area.

In Eqs. (1) and (2), the left side refers to the mass change and mass transfer caused by the flow of water and gas, respectively, while the right side refers to the mass change of water and gas due to hydrate dissociation. In Eq. (3), since the hydrate does not flow, unlike the gas and water phases, there is no flow term.

3.2. Heat transfer

3.2.1. Heat transfer in the geothermal layer and wellbore

The heat transfer in the geothermal layer and wellbore can be described as follows:

$$\frac{\partial T_f}{\partial t}=u_b\frac{\partial T_f}{\partial z}+\frac{2\pi r_{ti}U_{we}}{\rho_f C_f A_b}(T_{e,0}-T_f) \tag{4}$$

$$\rho_e C_e\frac{\partial T_e}{\partial t}=\frac{1}{r}\frac{\partial}{\partial r}\left(\lambda_e r\frac{\partial T_e}{\partial r}\right) \tag{5}$$

where T and C are the temperature and specific heat capacity, respectively; subscripts f and e denote the pore fluid and formation, respectively; u_b is the fluid flow velocity, in $m\cdot s^{-1}$; r is the distance to the wellbore center, in m; r_{ti} is the radius of the production pipe, in m; U_{we} is the comprehensive heat-transfer coefficient between the gas and the surrounding environment, in $W\cdot(m^2\cdot°C)^{-1}$; A_b is the area of the production pipe, in m^2; and λ_e is the heat conductivity of the formation, in $W\cdot(m^2\cdot°C)^{-1}$.

The left side of Eq. (4) refers to the energy change in the production pipe, and the right side refers to the energy change caused by the fluid flow and the heat transfer from the formation. The left side of Eq. (5) refers to the energy change in the formation, and the right side refers to the energy change caused by heat conduction.

3.2.2. A local thermal non-equilibrium model in hydrate-bearing sediments

The thermal characteristics of porous media containing hydrate phase transitions are highly complex, involving various forms of energy exchange and local thermal nonequilibrium effects. In this section, we develop a thermal model for the reservoir that accurately reflects the experimental and reservoir-scale conditions, while also considering significant heat-transfer mechanisms at the pore scale, such as solid–fluid thermal nonequilibrium effects and the Joule–Thomson effect induced by gas flow [40]. As an improvement on typical local thermal equilibrium models, we establish a fully coupled unsteady-state thermal model at the pore scale by accounting for multiple heat-flow forms associated with hydrate decomposition and gas–liquid flow. First, the heat-transfer mechanisms between the flow and solid phases in porous media are revealed, leading to the construction of an unsteady-state thermal model that incorporates the solid–fluid thermal nonequilibrium in porous media.

$$(\rho C)_{\mathrm{eh}}\frac{\partial\left[(1-\phi_{\mathrm{wg}})T_{\mathrm{e}}\right]}{\partial t}=\nabla\cdot\left[(1-\phi_{\mathrm{wg}})k_{\mathrm{eh}}\nabla T_{\mathrm{e}}\right]-\Delta H_{\mathrm{h}}\dot{m}_{\mathrm{h}}+h_{\mathrm{sf}}A_{\mathrm{sf}}(T_{\mathrm{f}}-T_{\mathrm{e}}) \tag{6}$$

$$\underbrace{\phi_{\mathrm{wg}}\left(\rho_{\mathrm{g}}S_{\mathrm{g}}C_{\mathrm{p,g}}+\rho_{\mathrm{w}}S_{\mathrm{w}}C_{\mathrm{p,w}}\right)\frac{\partial T_{\mathrm{f}}}{\partial t}}_{\text{Change in internalenergy}}=-\underbrace{\left(\rho_{\mathrm{g}}S_{\mathrm{g}}v_{\mathrm{g}}C_{\mathrm{p,g}}+\rho_{\mathrm{w}}S_{\mathrm{w}}v_{\mathrm{w}}C_{\mathrm{p,w}}\right)\nabla T_{\mathrm{f}}}_{\text{Energy transfer induced by fluid flow}}+\underbrace{\nabla\cdot(\phi_{\mathrm{wg}}k_{\mathrm{f}}\nabla T_{\mathrm{f}})}_{\text{Heat conduction}}+\underbrace{h_{\mathrm{sf}}A_{\mathrm{sf}}(T_{\mathrm{e}}-T_{\mathrm{f}})}_{\text{Convective heat transfer at boundaries}}+\underbrace{\rho_{\mathrm{g}}S_{\mathrm{g}}v_{\mathrm{g}}C_{\mathrm{p,g}}\mu_{\mathrm{JT}}\nabla p+\phi_{\mathrm{wg}}\rho_{\mathrm{g}}S_{\mathrm{g}}\mu_{\mathrm{JT}}C_{\mathrm{p,g}}\frac{\partial p}{\partial t}+\frac{\partial(\phi_{\mathrm{wg}}p)}{\partial t}}_{\text{Joule–Thomson effect}}-\underbrace{(C_{\mathrm{p,g}}\dot{m}_{\mathrm{g}}+C_{\mathrm{p,w}}\dot{m}_{\mathrm{w}})T_{\mathrm{e}}}_{\text{Enthalpy of the decomposing fluid}} \tag{7}$$

where $(\rho C)_{\mathrm{eh}}$ denotes the effective product of the solid phase density and specific heat capacity, in J·(m^3·°C)$^{-1}$, k_{eh} denotes the thermal conductivity of the solid phase, in W·(m·°C)$^{-1}$, where both can be calculated by the volume fraction weighted average of the hosting sediment and hydrate phase; ΔH_{h} is the heat of gas hydrate dissociation, in J·kg^{-1}; h_{sf} is the convection heat-transfer coefficient between the solid phase and the pore fluid, in W·(m^2·°C)$^{-1}$; A_{sf} is the specific surface area of the porous media, in m^{-1}; v_{g} and v_{w} are the flow velocities of gas and water, respectively, in m·s^{-1}; $C_{\mathrm{p,g}}$ and $C_{\mathrm{p,w}}$ are the specific heat capacities of gas and water, respectively, in J·(kg·°C)$^{-1}$; and μ_{jT} is the coefficient of the Joule–Thomson effect, in K·Pa^{-1}.

The left-hand side of Eq. (6) represents the change in the internal energy of the solid phase, while the terms on the right-hand side respectively represent the heat conduction between the solid phases, the heat absorbed by hydrate decomposition, and the interfacial convective heat transfer with the pore fluids. The left-hand side of Eq. (7) represents the change in the internal energy of the fluid phase, while the terms on the right-hand side respectively represent the energy transfer due to flow, heat conduction, interfacial convective heat transfer, Joule–Thomson effects, and enthalpy of the production fluids.

3.3. Hydrate dissociation

Selim and Sloan [41] described hydrate decomposition within porous media as a moving-front process under a fixed heat flux and subsequently incorporated the effects of heat transfer in their research. Kim et al. [42] conducted hydrate decomposition experiments within hydrate slurry systems and established the classic intrinsic decomposition kinetics model for hydrates (the K–B model). This model, which has been widely used in subsequent experimental studies and numerical simulations, is expressed as follows:

$$-\frac{\mathrm{d}n_{\mathrm{h}}}{\mathrm{d}t}=k_{\mathrm{d}}\exp\left(\frac{-\Delta E}{RT}\right)A_{\mathrm{h}}(f_{\mathrm{eq}}-f_{\mathrm{g}}) \tag{8}$$

where n_{h} is the number of moles of hydrate, in mol; k_{d} is the intrinsic reaction constant of the hydrate, in mol·(Pa·s)$^{-1}$·m^{-2}; ΔE is the activation energy of the hydrate, in J·mol^{-1}; R is the gas constant, in J·mol^{-1}·K^{-1}; A_{h} is the specific surface area for mass transfer during the hydrate phase transition, in m^{-1}; and f_{eq} and f_{g} are the fugacities of methane under hydrate phase equilibrium conditions and in the free gas phase, respectively, in Pa.

4. Results and discussion

The heat-extraction medium used in the proposed method could be seawater, CO_2, or other fluids. If CO_2 is used as the working fluid, the additional benefits of carbon storage should be considered to explore the economy of this method, as the field tests [14] indicated that the gas recovery rate of CO_2 exchange when mining hydrates can hardly reach the commercial gas production threshold. In addition, the negative impacts of pipe string corrosion caused by seawater and the precipitation of solid salt on gas production are worthy of attention. Therefore, this work selects fresh water, which has the most commercial potential, as the heat-extraction medium for the case study.

4.1. Evidence of the coexistence of geothermal energy and hydrate layers

The Shenhu area is located southeast of the Shenhu Shoal on the mid-slope of the northern South China Sea. It is bounded to the north by the Shenhu Uplift and Panyu Low Uplift and to the south by the Southern Uplift, making it part of the Zhu II Depression in the Pearl River Mouth Basin. This region lies in the transition zone between the continental and oceanic crusts, with a crustal thickness ranging from 18 to 24 km. The area features a series of depressions, including Shunde, Kaiping, Baiyun, and Liwan, forming a

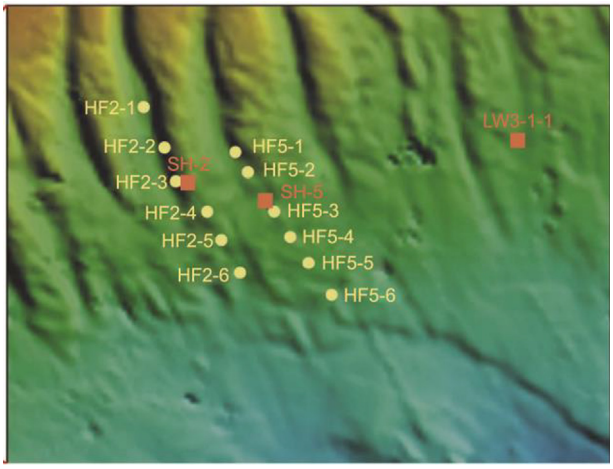

Fig. 2. Topography, geomorphology, and heat-flow measurement points in the Shenhu area. The orange squares represent drilling locations, and the yellow dots indicate heat-flow measurement points.

northeast-trending rift zone. The northern South China Sea slope region is characterized by East–Northeast-, Northeast-, or Northwest-trending faults (Fig. 2). The former are extensional faults, while the latter are viewed as extensional-shear faults, both of which exhibit good water conductivity.

Late-stage faulting in Shenhu area is extremely rich, with increasingly developed Cenozoic faults from the bottom upward. The faults at the base of the Paleogene were the main controlling factors during the rift stage deposition. Basal faulting activity intensified during the thermal subsidence, peaking between 2.0 and 1.5 Ma in the Pliocene, resulting in a highly permeable fractured medium conducive to extensive deep fluid flow and hydrate development. Following fault activity, the seafloor of the Shenhu area experienced rapid sediment deposition (10–20 $cm{\cdot}ka^{-1}$). These new sediments remain unconsolidated, showing fewer fracture traces. Neotectonic modifications have created numerous late-stage structural traps and large-scale mud diapir belts, which are believed to be closely related to the gas hydrate development in the Shenhu area. The complex fault activity and rapid sedimentation have facilitated the formation of permeable pathways and traps, promoting the extensive development of NGHs.

The drilling area, which is located between the Shenhu Shoal and the Dongsha Islands, features a complex seabed topography. The general trend of the seabed slopes from north to south, with gradually increasing water depths (Fig. 2). The seafloor exhibits diverse geomorphological features, including sea mounds, sea valleys, erosion gullies, reverse slope terraces, and submarine trenches. Moreover, the drilling area is characterized by a high sedimentation rate, numerous faults, and well-developed mud diapirs, which facilitate fluid migration. These conditions create a favorable environment for the large-scale formation of NGH reservoirs.

In recent years, extensive heat-flow measurements have been conducted along the northern continental margin of the South China Sea (Fig. 2). These data indicate that this region has a high heat-flow background. The heat-flow values in the gas hydrate drilling area range from 56 to 101 $mW{\cdot}m^{-2}$, with most stations recording values above 75 $mW{\cdot}m^{-2}$. However, in the wells where hydrates have been discovered (SH2, SH3, and SH7), the heat-flow values range from 65 to 70 $mW{\cdot}m^{-2}$—significantly lower than the overall heat-flow field of the Shenhu area.

The formation of the local topography involves rapid sedimentation due to slumping and a bottom current erosion that forms erosion valleys. Additionally, faults, fractures, or diapirs representing fluid-discharge pathways often develop beneath these erosion valleys and gullies. Periodic fluid activity can locally alter the geothermal gradient. The interplay of these factors results in significant heat-flow variations over a relatively small area in this region.

To investigate the geothermal characteristics of the gas hydrate reservoirs, the Guangzhou Marine Geological Survey conducted intensive seabed heat-flow measurements within a 2 km radius around well SH2. The results indicated significant fluctuations in the measured heat-flow values, ranging from 48.4 to 111.5 $mW{\cdot}m^{-2}$. In contrast, the heat-flow values calculated from the seismic reflection profile of a bottom simulating reflector (BSR) showed less variation, ranging from 65.7 to 75.3 $mW{\cdot}m^{-2}$. This discrepancy suggests that subsurface hydrothermal circulation significantly influences the measured heat-flow values, resulting in numbers that deviate substantially from other data sources.

Based on the measured seabed heat flow and BSR heat-flow results, an average heat flow of 70 $mW{\cdot}m^{-2}$ was adopted for the present study. The average thermal conductivity of the sedimentary layers in the northern South China Sea is approximately 1.26 $W{\cdot}(m{\cdot}K)^{-1}$, with a heat-generation rate of about 1.34 $\mu W{\cdot}m^{-3}$. Consequently, the calculated geothermal gradient is approximately 0.054 $°C{\cdot}m^{-1}$. This result provides substantial evidence for the coexistence of gas hydrate reservoirs and geothermal layers at different depths within the same location in the South China Sea.

4.2. Geothermal energy exploitation characteristics

Here, we take the hydrate reservoir in the Shenhu area of the South China Sea as an example. The vertical depth of the geothermal well is 4000 m, with the following wellbore structure: 21-inch riser × 1225 m + 26-inch casing × 2200 m + $12\frac{1}{4}$-inch casing × 3400 m + $9\frac{5}{8}$-inch casing × 4000 m + $8\frac{1}{2}$-inch horizontal open hole × 3000 m (1 inch = 0.0254 m). The wellbore structure for the hydrate production/injection well is as follows: 30-inch riser × 1225 m + 26-inch casing × 1286.8 m + $12\frac{1}{4}$-inch casing × 1512.7 m + $9\frac{5}{8}$-inch casing × 2121.23 m. The other important parameters used in the simulation, such as the physical properties of the reservoir, initial temperature and pressure distribution, wellbore parameters, and thermal properties, are summarized from relevant studies in Table 1 [16,18].

4.2.1. Wellbore temperature evolution

Fig. 3 depicts the temperature profile distribution within the borehole of a U-shaped well used for thermal extraction. Along the depth of the well, water is injected from the platform wellhead; it passes through cooler seawater sections and shallow layers, resulting in an initial decrease in temperature. However, as the formation temperature increases, the direction of heat exchange reverses, transferring heat from the formation to the borehole and causing a gradual rise in fluid temperature. Upon entering the horizontal section within the geothermal layer, the fluid temperature increases rapidly. The simulation indicates that 85.21% of the thermal energy acquired by the fluid is sourced from the deep high-temperature geothermal layer, with the heat-extraction efficiency improving with an increase in horizontal section length. As the water enters the production well, the temperature of the deep formation exceeds that of the water, leading to a continued rise in borehole temperature. Upon returning to the upper part of the borehole, the fluid begins to release energy back into the formation, resulting in a gradual decrease in temperature and an energy loss of approximately 9.74%.

Fig. 4 illustrates the temporal variation in temperature as the fluid enters the hydrate layer. As shown in the Fig. 4, during the initial phase of extraction (the first year), the temperature of the heated water decreases significantly (approximately 9 °C per year). This decline is primarily attributed to the low thermal conductivity of the rock, which limits the rapid transfer of energy from the surrounding formation to the borehole. Consequently, the temperature in the near-borehole formation experiences a marked decrease during this initial period. However, as the temperature in the near-borehole zone decreases, the internal temperature gradient within the formation increases, thereby increasing the thermal conductivity [43]. As a result, the rate of temperature decline in the borehole gradually slows. After approximately five years, a

Table 1
Main parameters of the gas production from the hydrate reservoir [16,18].

Parameter	Value
Water depth	1225 m
Injection pressure	16.5 MPa
Porosity of hydrate layer	0.373
Permeability of hydrate layer	2.38 mD
Depth of the geothermal layer	4000 m
Production pressure	3.0 MPa
Saturation of hydrate layer	0.31
Thickness of hydrate layer	45 m

1 mD = 10^{-3} μm^2.

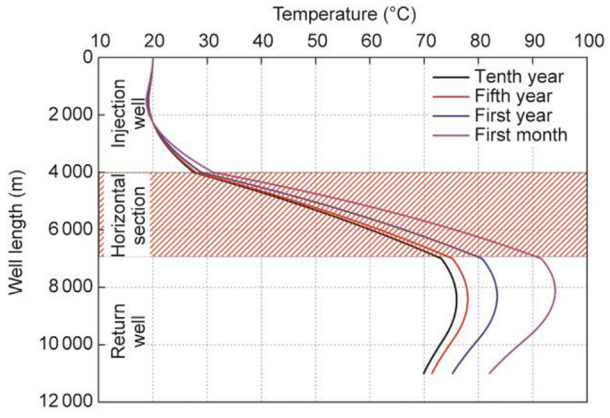

Fig. 3. Temperature profiles in the heat recovery well system at first month, first year, fifth year, and tenth year.

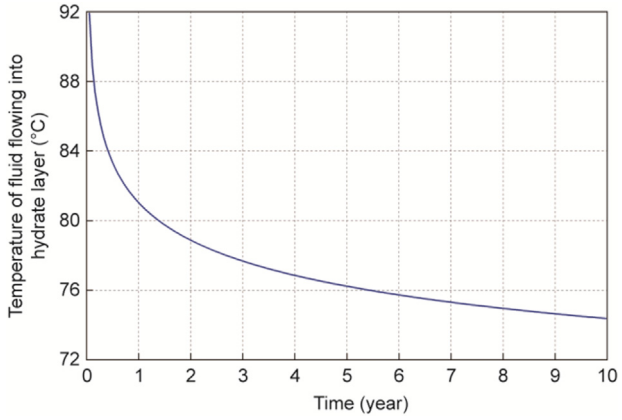

Fig. 4. Variation in the temperature of the fluid flowing into the hydrate layer over time.

quasi-steady state is observed, with temperatures continuing to decrease at an annual rate of about 0.4 °C.

4.2.2. Fluid production behaviors

The hydrate-extraction strategy employed in the foundational example involves the initial use of dual horizontal wells for depressurization extraction, allowing for the optimal utilization of the inherent geothermal energy of the formation. After one year of depressurization production, one of the production wells is converted into a thermal injection well, facilitating a combined development approach that leverages both geothermal energy and depressurization.

Fig. 5 illustrates the variations in the gas production rates and cumulative gas output over an 8-year production cycle. The data indicate that the gas production rate follows a pattern of initial increase followed by a decrease, characterized by two distinct phases of change. Based on the inflection points in the gas production rate trend, the entire hydrate development process can be subdivided into five stages:

(1) **Initial depressurization period (0–50 d)**. During this period, the reservoir is newly opened, and the formation energy—along with the hydrates in the near-borehole zone—is abundant. Consequently, along with the progress in depressurization, the gas production rate gradually increases, peaking at approximately 4.50×10^4 $m^3 \cdot d^{-1}$ after 50 d.

(2) **Residual depressurization period (50 d–1 a)**. As the hydrates in the near-borehole zone fully decompose and the formation temperature decreases, combined with the extremely low permeability of the clayey siltstone-dominated hydrate reservoir, the depressurization effect becomes significantly limited. This leads to a sharp decline in both hydrate decomposition and natural gas production rates.

(3) **Pre-thermal injection period (1.0–2.6 a)**. After the first year, thermal injection commences in conjunction with depressurization. At the outset of this phase, one of the production wells was converted to an injection well, resulting in a sharp drop in the gas production rate, which continues to decline until it reaches a trough of approximately 0.35×10^4 $m^3 \cdot d^{-1}$ at around 2.6 a. During the depressurization production phase, the hydrates in the near-borehole zone are either almost fully decomposed or possess very low saturation. As a result, the impact of the thermal water on increasing the hydrate decomposition is limited before it reaches the deeper reservoir with higher hydrate saturation. In addition, the distance between two wells is 150 m, so the gas generated from decomposition around the injection well has not yet been displaced to the production well by water. Consequently, the initial phase of thermal injection has a minimal effect on increasing the gas production rate, which continues to decline gradually, albeit at a slowing rate.

(4) **Mid-thermal injection period (2.6–6.1 a)**. During this period, a substantial amount of thermal water is injected into the hydrate reservoir, resulting in significant gas generation that is subsequently displaced into the production well. As a result, the gas production rate gradually begins to rise. After approximately 2.66 a, the gas production rate from combined method surpasses that of the pure depressurization method, peaking at around 1.09×10^4 $m^3 \cdot d^{-1}$ by 6.1 a.

(5) **Late thermal injection period (6.1–8.0 a)**. As the hydrates within the thermal injection zone are nearly completely decomposed, the gas production rate begins to decline slowly until complete decomposition of the hydrates throughout the reservoir is achieved.

From the cumulative gas production curve, it is evident that the cumulative gas output of the proposed method surpasses those of the pure depressurization method and the homocentric-squared well system after 3.34 years [34]. Over the 8-year production cycle, the cumulative natural gas outputs for the pure depressurization method and the homocentric-squared well system are 1.83166×10^7 and 2.10641×10^7 m^3, respectively, while the cumulative gas output for the proposed method reaches 3.16090×10^7 m^3, representing improvements of 72.57% and 50.06% compared with the pure depressurization method and the homocentric-squared well system, respectively.

Fig. 6 illustrates the variations in water production rate and cumulative water output over the 8-year production cycle. As shown, the water production pattern of the proposed method is inversely related to the gas production pattern, exhibiting a trend of initial decline, followed by an increase, then a subsequent decrease, and finally another increase. Although injecting thermal water into the hydrate reservoir increases the individual well's water production rates (with an average increase of 36.51%), the pure depressurization method utilizing dual wells achieves a higher total water production rate. Over an 8-year production cycle, the cumulative water output for the pure depressurization method is 2.2298×10^6 m^3, whereas that for the proposed method is only 1.5219×10^6 m^3, representing a decrease of 31.75%.

To sum up, compared with the pure depressurization method, the production process of utilizing dual horizontal wells for the combined geothermal energy and depressurization extraction of hydrates demonstrates significant advantages over an 8-year production cycle. Specifically, it achieves a 72.57% increase in cumulative gas production while reducing the cumulative water production by 31.75%. These results indicate that this new method

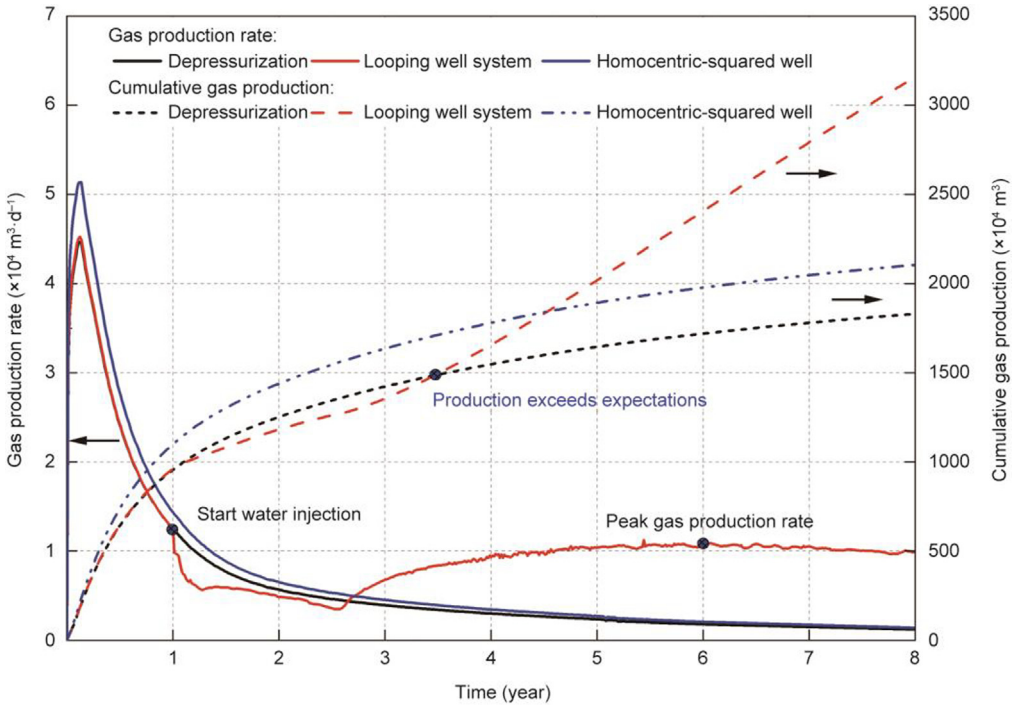

Fig. 5. Evolution of gas production rate and cumulative gas production during the hydrate production period. The homocentric-squared well system is a hydrate production well structure similar to a looping well system. Its specific structure is shown in Ref. [34]. A homocentric squared well includes only a heat-extraction well and gas production well. The fluid gains geothermal energy from the deep formations and returns to the production well. The heat is transferred to the hydrate-bearing sediments through convection heat transfer in the production well, instead of injecting water into the hydrate-bearing sediments.

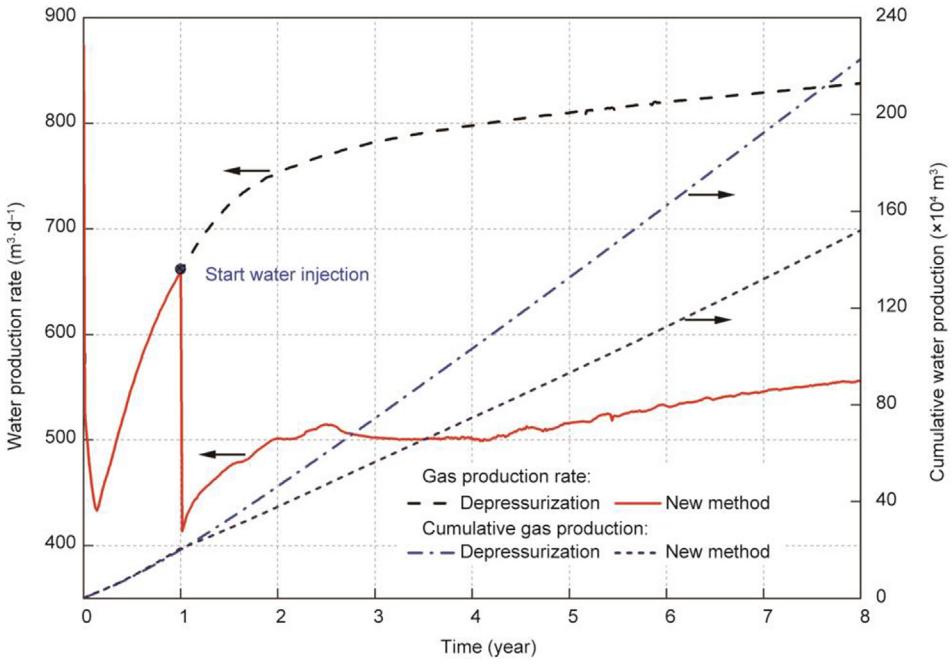

Fig. 6. Evolution of the water production rate and cumulative water production during the hydrate production period.

represents a substantial advancement over existing techniques, highlighting its potential feasibility for commercial development.

The injection flow rate of the loop well system determines the fluid temperature in the hydrate reservoir, thereby influencing the kinetics of hydrate decomposition. Fig. 7 presents the temperature variations of the fluid in the hydrate reservoir under different thermal fluid-injection rates. It is important to note that the flow rate referenced here represents the circulation volumetric flow rate of water within the dual horizontal well system, which does not have a direct correlation with the flow rate of the fluid injected into the hydrate reservoir. As illustrated in the figure, a higher injection flow rate results in a lower fluid temperature upon entering the hydrate reservoir. This phenomenon primarily occurs because a greater flow rate reduces the heat-exchange duration

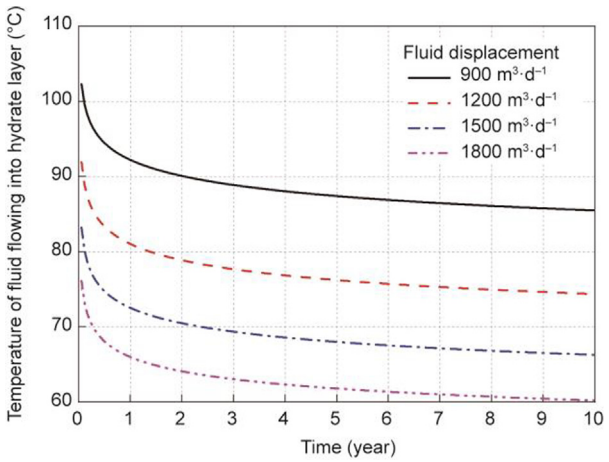

Fig. 7. Temperature variation in the fluid flowing into the hydrate layer at different fluid rates.

within the geothermal layer's horizontal well, leading to a lower fluid temperature. When the flow rate increases from 900 to 1800 $m^3 \cdot d^{-1}$, the average temperature of the fluid decreases from 88.33 to 62.62 °C, for a reduction of approximately 29.11%.

Fig. 8 illustrates the variations in the gas production rates and cumulative gas output under different thermal fluid-injection rates. It is evident that the differences in fluid temperature lead to variations in the gas production rates within the reservoir, although these differences are relatively minor. The daily average gas production rates for the four injection rates are 0.807, 0.832, 0.861, and 0.894 million $m^3 \cdot d^{-1}$, respectively. As the average injection temperature increases from 62.62 to 88.33 °C, the average gas production rate during the 7-year thermal extraction period rises by 10.66%, while the cumulative gas output over the 8-year production cycle increases by 7.27%.

These findings confirm that significantly increasing the temperature of the injected fluid does not substantially increase the gas production rate. This limitation arises because much of the energy from the injected fluid is utilized to elevate the formation temperature and is lost through the outer boundaries, with only a small proportion being dedicated to enhancing the kinetics of hydrate decomposition. Therefore, in practical hydrate-extraction processes, it is unnecessary to pursue excessively high injection temperatures. Specifically, for a threshold temperature of 62 °C, an onsite geological depth of about 4000 m (with a formation temperature of ~140 °C) is expected to realize the optimal economic

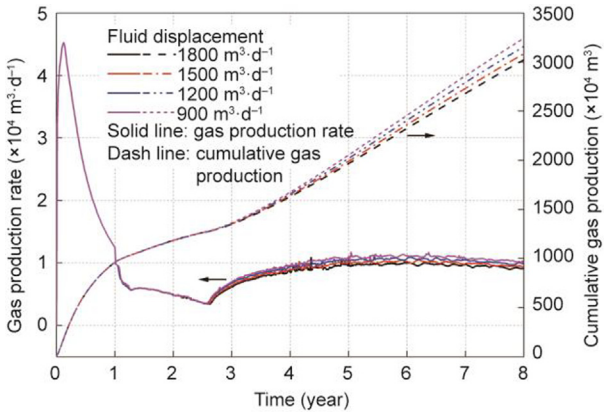

Fig. 8. Evolution of the gas production rate and cumulative gas production with different fluid displacements.

exploitation of NGHs, as the limited gas production increase cannot offset the high drilling costs. Of course, this threshold temperature is determined by the burial depth, saturation, porosity, and other characteristics of the hydrate-bearing sediments, which vary under different geological conditions.

4.3. Commercialization potential

Longer horizontal sections lead to faster gas production rates; however, this also results in higher drilling and completion costs. Research by Walsh et al. [44] and Deepak et al. [45] indicated that drilling and completion costs make up the most significant portion of the overall expenditures in hydrate production projects, typically accounting for 20%–50% of the total costs. However, these costs would be influenced by various factors, including the geographical location, reservoir lithology, and drilling technology, resulting in considerable cost variability. Moreover, there is a lack of publicly available data from companies regarding actual costs. Therefore, this study employs the empirical predictive model developed by Lukawski et al. [46], based on terrestrial drilling and completion cost survey data:

$$C_{won} = 1.172 \times 10^{-7}(\text{MUSD} \cdot \text{m}^{-2})H^2 + 2.3 \times 10^{-3}(\text{MUSD} \cdot \text{m}^{-1})H - 0.62(\text{MUSD}) \quad (9)$$

where C_{won} represents the terrestrial drilling and completion cost in million USD (MUSD), and H denotes the well depth in m.

Compared with terrestrial drilling, offshore drilling incurs higher costs due to the harsh conditions of deep-sea environments, which typically correlate positively with the water depth. Based on the available data, Kaiser [47] estimated that deep-sea conditions result in a cost increase of approximately $0.006H_w$, where H_w represents the water depth in m. In addition, the drilling costs for horizontal sections are higher than those for vertical sections. Research by Lei et al. [48] indicated that the drilling cost for a horizontal section is approximately 1.5–2.5 times greater than that of a vertical section; for this analysis, we use a factor of 2. Thus, the rough estimation formula for the drilling and completion costs of a hydrate reservoir in a marine environment is expressed as follows:

$$C_{whye} = 0.006(\text{MUSD} \cdot \text{m}^{-1})H_w + C_{won} + 2\frac{H_h}{H}C_{won} \quad (10)$$

where C_{whye} is the drilling and completion cost of a hydrate reservoir in the sea, in MUSD; and H_h is the length of the horizontal section, in m.

It is worth noting that exploration costs, equipment costs (the subsea production manifold and the gas production platform and equipment), and operating costs are also included in the hydrate production process, along with the drilling and completion costs. Among them, exploration costs and equipment costs are fixed early-stage inputs and are basically not affected by natural gas production capacity. Certainly, this part of the cost is usually for a hydrate reservoir block, and the fixed investment in the early stage of a single injection production system needs to be divided by the cost-sharing coefficient, which is temporarily set to 100 in this work. Therefore, based on research results on early investment in hydrate mining carried out by Walsh et al. [44] and Deepak et al. [45], we set the early investment in hydrate mining at 13.65 MUSD. The operating costs are greatly affected by the natural gas production capacity. Since there are no current cases of the commercial development of a hydrate reservoir, this work roughly assumes that this part of the cost is consistent with previous experience with drilling and completion costs.

Taking the hydrate deposit from the second trial production site in the South China Sea as an example, Fig. 9 illustrates the variations in average gas production rate, total development costs,

and unit costs of produced natural gas with changes in horizontal well length. It is evident that the total development costs increase exponentially with horizontal well length, resulting in a trend in which the unit cost of the produced natural gas initially decreases and then increases. When the horizontal section length is below 800 m, the unit cost of the produced natural gas decreases rapidly (from 4.99 USD·m^{-3} at 100 m to 0.89 USD·m^{-3} at 800 m). At a horizontal well length of 2010 m, the average gas production rate reaches 5.41 × 10^4 m^3·d^{-1}, with the lowest unit cost of the produced natural gas at approximately 0.66 USD·m^{-3}. This price is still significantly higher than the ex-factory price of finished liquefied natural gas (LNG) on the market (0.55 USD·m^{-3} in China, as of August 2024).

However, as a regional energy source, natural gas is significantly influenced by market structures, resulting in substantial price fluctuations. The prices for residential natural gas range between 0.25 and 0.48 USD·m^{-3}. Additionally, with the rapid advancement of drilling technologies and techniques, as well as the maturation of the "well factory" production model, drilling and production operational costs are expected to further decrease.

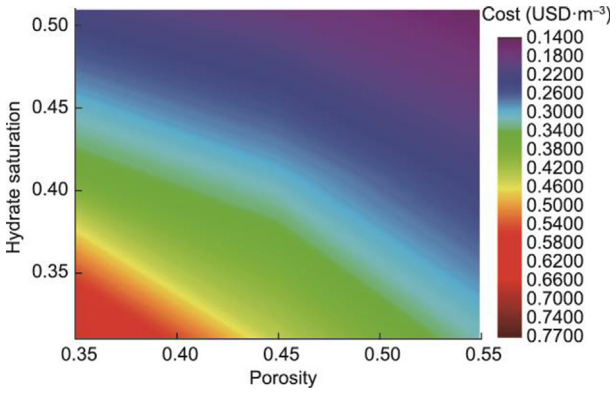

Fig. 9. Variation in the average gas production rate, total cost, and unit cost of natural gas with the length of the horizontal well.

Research indicates that, if the cost of hydrate development can be reduced by 30%, the average price of produced natural gas could fall to about 0.46 USD·m^{-3} at the optimal horizontal section length, which is slightly below the current peak price of residential natural gas.

Fig. 10 illustrates the unit costs of produced natural gas under varying porosity and hydrate saturation levels. It is evident that the average price of the produced natural gas decreases with increasing porosity and hydrate saturation. If the reservoir porosity reaches 0.55 and the saturation level reaches 0.51, by utilizing the proposed dual horizontal well method for hydrate development (with a 2010-m horizontal production well), the average gas production rate can reach 2.457 × 10^5 m^3·d^{-1}, and the unit cost of the produced natural gas can be reduced to about 0.14 USD, indicating potential for the commercial development of hydrate resources.

In summary, although the proposed dual horizontal well significantly increases gas production rates for the hydrate deposits discovered in the Shenhu area of the South China Sea, it has not yet reached the production threshold necessary for commercial development. The geological conditions of the hydrate-bearing segments are still important factors determining the commercial development of the hydrate. However, if future efforts can reduce the cost inputs by more than 30%, or if geologically favorable hydrate reservoirs (with a porosity > 0.5 and hydrate saturation > 0.5) are identified, along with the establishment of kilometer-scale horizontal production wells, our proposed method and supporting production technologies can greatly increase the likelihood of achieving the commercial development of hydrate resources.

5. Conclusions

To advance the commercial development of hydrate resources in the South China Sea, this study proposed a new method for hydrate extraction that utilizes geothermal energy and depressurization through dual horizontal wells. This method addresses key scientific issues, including the dynamics of hydrate decomposition

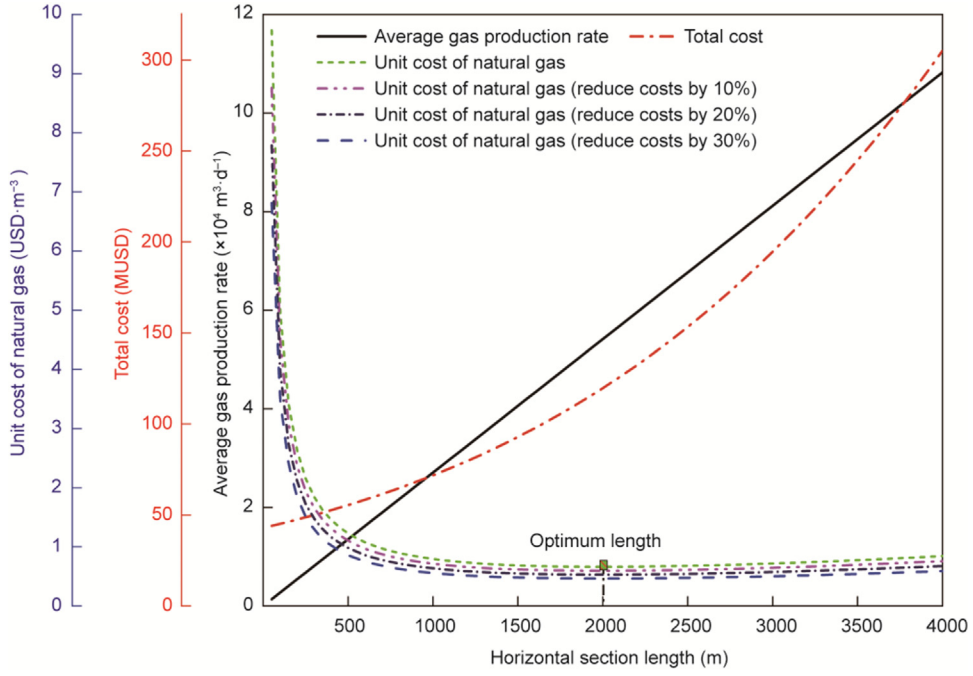

Fig. 10. Unit cost of natural gas at different porosities and hydrate saturations.

within porous media, the unsteady heat-transfer mechanisms in porous media, and the coupling mechanism of mass and heat transfer among the wellbore, geothermal layer, and hydrate layer. A comprehensive mathematical model was developed, leading to the following significant advancements:

(1) As the temperature of fluids from the geothermal layer exceeds approximately 62 °C, the fluid heat is mainly consumed by the rock matrix of the hydrate formation, instead of promoting NGH dissociation. As a result, common geothermal gradient formation can be used effectively to exchange geothermal energy.

(2) Compared with traditional depressurization methods, the proposed method achieves a 72.57% increase in cumulative gas production and a 31.75% reduction in cumulative water production over an 8-year production period in the Shenhu area of the South China Sea.

(3) Taking the hydrate deposits in the South China Sea as an example, when the horizontal section length of the production well is 2010 m, the unit cost of the produced natural gas is minimized. If the costs associated with hydrate development can be reduced by 30%, the unit cost of the produced natural gas could theoretically decrease to about 0.46 USD·m^{-3}, which is slightly below the current peak price for residential natural gas.

(4) If geologically favorable hydrate reservoirs (with porosity > 0.5 and hydrate saturation > 0.5) can be identified, and if 2000 m horizontal production wells can be established using the proposed method, the unit cost of the produced natural gas could further decrease to approximately 0.14 USD·m^{-3}, indicating potential for the commercial development of hydrates.

CRediT authorship contribution statement

Baojiang Sun: Writing – review & editing, Validation, Supervision. **Jinsheng Sun:** Validation, Supervision, Investigation. **Youqiang Liao:** Writing – original draft, Visualization, Software, Methodology, Investigation. **Miao Dong:** Validation, Investigation. **Jie Zhong:** Writing – original draft, Methodology. **Praveen Linga:** Writing – review & editing, Supervision.

Declaration of competing interest

The authors declare that they have no known competing financial interests or personal relationships that could have appeared to influence the work reported in this paper.

Acknowledgments

This work was supported by the National Natural Science Foundation of China (52288101, 51991360, and U21B2069).

References

[1] Sloan ED. Fundamental principles and applications of natural gas hydrates. Nature 2003;426:353–63.
[2] Chong Z, Yang S, Babu P, Linga P, Li X. Review of natural gas hydrates as an energy resource: prospects and challenges. Appl Energy 2016;162:1633–52.
[3] Zhang X, Gao Z, Zhou B, Guo H, Xu Y, Ding Y, et al. Advanced compressed air energy storage systems: fundamentals and applications. Engineering 2024;34:246–69.
[4] Rui Z, Zeng L, Dindoruk B. Challenges in the large-scale deployment of CCUS. Engineering 2024;44:17–20.
[5] Chen X, Yang J, Gao D, Hong Y, Zou Y, Du X. Unlocking the deepwater natural gas hydrate's commercial potential with extended reach wells from shallow water: review and an innovative method. Renew Sustain Energy Rev 2020;134:110388.
[6] Cook PJ. CCS research development and deployment in a clean energy future: lessons from Australia over the past two decades. Engineering 2017;3:477–84.
[7] Wan QC, Si H, Li B, Yin ZY, Gao Q, Liu S, et al. Energy recovery enhancement from gas hydrate based on the optimization of thermal stimulation modes and depressurization. Appl Energy 2020;278:115612.
[8] Ruan X, Li XS. Investigation of the methane hydrate surface area during depressurization-induced dissociation in hydrate-bearing porous media. Chinese J Chem Eng 2021;32:324–34.
[9] Stanwix PL, Rathnayake NM, de Obanos FPP, Johns ML, Aman ZM, May EF. Characterising thermally controlled CH_4–CO_2 hydrate exchange in unconsolidated sediments. Energy Environ Sci 2018;11:1828–40.
[10] Zhong X, Pan D, Zhu Y, Wang Y, Tu G, Nie S, et al. Commercial production potential evaluation of injection–production mode for CH-Bk hydrate reservoir and investigation of its stimulated potential by fracture network. Energy 2022;239:122113.
[11] Guo X, Xu L, Wang B, Sun L, Liu Y, Wei R, et al. Optimized gas and water production from water-saturated hydrate-bearing sediment through stepwise depressurization combined with thermal stimulation. Appl Energy 2020;276:115438.
[12] Li XS, Xu CG, Zhang Y, Ruan XK, Li G, Wang Y. Investigation into gas production from natural gas hydrate: a review. Appl Energy 2016;172:286–322.
[13] Tomaru H, Fehn U, Lu Z, Matsumoto R. Halogen systematics in the Mallik 5L-38 gas hydrate production research well, Northwest Territories, Canada: implications for the origin of gas hydrates under terrestrial permafrost conditions. Appl Geochem 2007;22:656–75.
[14] Hunter RB, Collett TS, Boswell R, Anderson BJ, Digert SA, Pospisil G, et al. Mount Elbert gas hydrate stratigraphic test well, Alaska north slope: overview of scientific and technical program. Marine Pet Geo 2011;28:295–310.
[15] Yamamoto K. Overview and introduction: pressure core-sampling and analyses in the 2012–2013 MH21 offshore test of gas production from methane hydrates in the eastern Nankai Trough. Marine Pet Geo 2015;66:296–309.
[16] Yu T, Guan G, Abudula A. Production performance and numerical investigation of the 2017 offshore methane hydrate production test in the Nankai Trough of Japan. Appl Energy 2019;251:113338.
[17] Ye J, Qin X, Xie W, Lu H, Ma B, Qiu H, et al. The second natural gas hydrate production test in the South China Sea. China Geo 2020;3:197–209.
[18] Qin X, Liang Q, Ye J, Yang L, Qiu H, Xie W, et al. The response of temperature and pressure of hydrate reservoirs in the first gas hydrate production test in South China Sea. Appl Energy 2020;278:115649.
[19] Zhou S, Zhao J, Li Q, Chen W, Zhou J, Wei N, et al. Optimal design of the engineering parameters for the first global trial production of marine natural gas hydrates through solid fluidization. Nat Gas Ind B 2018;5:118–31.
[20] Li J, Ye J, Qin X, Qiu H, Wu N, Lu H, et al. The first offshore natural gas hydrate production test in South China Sea. China Geo 2018;1:5–16.
[21] Wan QC, Si H, Li B, Li G. Heat transfer analysis of methane hydrate dissociation by depressurization and thermal stimulation. Int J Heat Mass Trans 2018;127:206–17.
[22] Yu T, Guan G, Abudula A, Wang D. 3D visualization of fluid flow behaviors during methane hydrate extraction by hot water injection. Energy 2019;188:116110.
[23] Yang M, Zhao J, Zheng J, Song Y. Hydrate reformation characteristics in natural gas hydrate dissociation process: a review. Appl Energy 2019;256:113878.
[24] Meng Y, Han B, Wang J, Chu J, Yao H, Zhao J, et al. Hydrate blockage in subsea oil/gas pipelines: characterization, detection, and engineering solutions. Engineering 2024;46:363–82.
[25] Zhao E, Hou J, Du Q, Liu Y, Ji Y, Bai Y. Numerical modeling of gas production from methane hydrate deposits using low-frequency electrical heating assisted depressurization method. Fuel 2021;290:120075.
[26] Li G, Li XS, Li B, Wang Y. Methane hydrate dissociation using inverted five-spot water flooding method in cubic hydrate simulator. Energy 2014;64:298–306.
[27] Li XS, Wang Y, Duan LP, Li G, Zhang Y, Huang NS, et al. Experimental investigation into methane hydrate production during three-dimensional thermal huff and puff. Appl Energy 2012;94:48–57.
[28] Liu S, Zhang Y, Luo Y, Liang Y, Li B. Analysis of hydrate exploitation by a new *in-situ* heat generation method with chemical reagents based on heat utilization. J Cleaner Prod 2020;249:119399.
[29] Liu Y, Hou J, Zhao H, Liu X, Xia Z. Numerical simulation of simultaneous exploitation of geothermal energy and natural gas hydrates by water injection into a geothermal heat exchange well. Renew Sustain Energy Rev 2019;109:467–81.
[30] Zeng L, Sander R, Chen Y, Xie Q. Hydrogen storage performance during underground hydrogen storage in depleted gas reservoirs: a review. Engineering 2024;40:211–25.
[31] Guo X, Hu D, Li Y, Duan J, Zhang X, Fan X, et al. Theoretical progress and key technologies of onshore ultra-deep oil/gas exploration. Engineering 2019;5:458–70.
[32] Li B, Zhang P, Zhu X, Zhang W, Dong L. Numerical analysis of nonlinear buckling response of a axially movable constrained drill string in horizontal wells with complex structures. Geoenergy Sci Eng 2024;241:213147.
[33] Majid AAA, Wu DT, Koh CA. A perspective on rheological studies of gas hydrate slurry properties. Engineering 2018;4:321–9.
[34] Sun B, Chen Y, Wang Z, Chen L, Gao Y, Xu J, et al. Homocentric squares-shaped well structure for marine hydrate reserve recovery utilizing geothermal heat and method thereof. United States patent US 201816058623. 2019 Apr 23.
[35] Choi JH, Myshakin EM, Lei L, Kneafsey TJ, Seol Y. An experimental system and procedure of unsteady-state relative permeability test for gas hydrate-bearing sediments. J Nat Gas Sci Eng 2020;83:103545.
[36] Dai S, Kim J, Xu Y, Waite WF, Jang J, Yoneda J, et al. Permeability anisotropy and relative permeability in sediments from the National Gas Hydrate Program Expedition 02, offshore India. Marine Pet Geo 2019;108:705–13.
[37] Liao Y, Sun X, Sun B, Wang Z, Zhang J, Lou W. Wellhead backpressure control strategies and outflow response characteristics for gas kick during managed pressure drilling. J Nat Gas Sci Eng 2020;75:103164.

[38] Cui G, Ren S, Zhang L, Ezekiel J, Enechukwu C, Wang Y, et al. Geothermal exploitation from hot dry rocks via recycling heat transmission fluid in a horizontal well. Energy 2017;128:366–77.
[39] Pan L, Freifeld B, Doughty C, Zakem S, Sheu M, Cutright B, et al. Fully coupled wellbore-reservoir modeling of geothermal heat extraction using CO_2 as the working fluid. Geothermics 2015;53:100–13.
[40] Liao Y, Zheng J, Wang Z, Sun B, Sun X, Linga P. Modeling and characterizing the thermal and kinetic behavior of methane hydrate dissociation in sandy porous media. Appl Energy 2022;312:118804.
[41] Selim MS, Sloan ED. Heat and mass transfer during the dissociation of hydrates in porous media. AIChE J 1989;35:1049–52.
[42] Kim HC, Bishnoi PR, Heidemann RA, Rizvi SSH. Kinetics of methane hydrate decomposition. Chem Eng Sci 1987;42:1645–53.
[43] Shaik AR, Rahman SS, Tran NH, Tran T. Numerical simulation of fluid–rock coupling heat transfer in naturally fractured geothermal system. Appl Thermal Eng 2011;31:1600–6.
[44] Walsh MR, Hancock SH, Wilson SJ, Patil SL, Moridis GJ, Boswell R, et al. Preliminary report on the commercial viability of gas production from natural gas hydrates. Energy Econom 2009;31:815–23.
[45] Deepak M, Kumar P, Singh K, Yadav US. Techno-economic forecasting of a hypothetical gas hydrate field in the offshore of India. Marine Pet Geo 2019;108:741–6.
[46] Lukawski MZ, Anderson BJ, Augustine C, Capuano LE, Beckers KF, Livesay B, et al. Cost analysis of oil, gas, and geothermal well drilling. J Pet Sci Eng 2014;118:1–14.
[47] Kaiser MJ. Modeling the time and cost to drill an offshore well. Energy 2009;34:1097–112.
[48] Lei Z, Zhang Y, Zhang S, Fu L, Hu Z, Yu Z, et al. Electricity generation from a three-horizontal-well enhanced geothermal system in the Qiabuqia geothermal field, China: slickwater fracturing treatments for different reservoir scenarios. Renew Energy 2020;145:65–83.